Animatable 3D Gaussians for High-fidelity Synthesis of Human Motions

Keyang Ye Tianjia Shao Kun Zhou
State Key Lab of CAD&CG, Zhejiang University
yekeyang@zju.edu.cn, tjshao@zju.edu.cn, kunzhou@acm.org

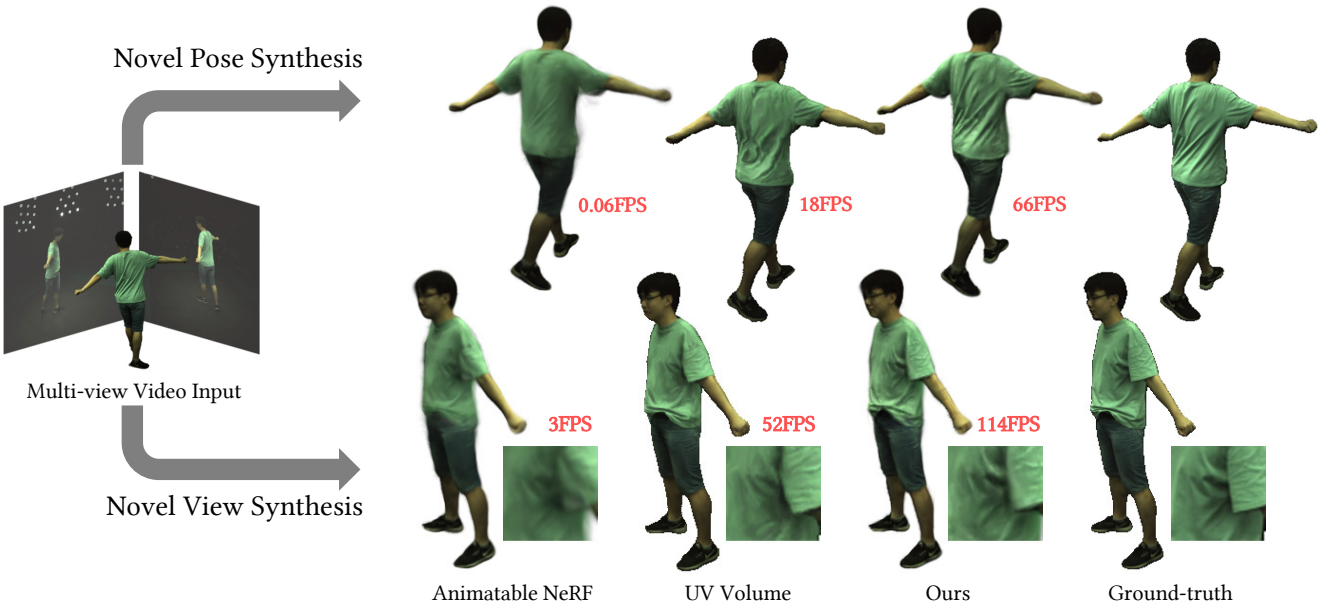

Figure 1. Given a multi-view video of a performer, our method reconstruct an animatable human represented by 3D Gaussians. By decoding pose-dependent appearances via a tiny MLP, our method achieves high-fidelity real-time novel view and novel pose synthesis.

Abstract

We present a novel animatable 3D Gaussian model for rendering high-fidelity free-view human motions in real time. Compared to existing NeRF-based methods, the model owns better capability in synthesizing high-frequency details without the jittering problem across video frames. The core of our model is a novel augmented 3D Gaussian representation, which attaches each Gaussian with a learnable code. The learnable code serves as a pose-dependent appearance embedding for refining the erroneous appearance caused by geometric transformation of Gaussians, based on which an appearance refinement model is learned to produce residual Gaussian properties to match the appearance in target pose. To force the Gaussians to learn the foreground human only without background interference, we further design a novel alpha loss to explicitly constrain the Gaussians within the human body. We also propose to jointly optimize the human joint parameters to improve the appearance accuracy. The animatable 3D Gaussian model can be learned with shallow MLPs, so new human motions can be synthesized in real time (66 fps on avarage). Experiments show that our model has superior performance over NeRF-based methods.

1. Introduction

Synthesizing photorealistic human animations is a key problem in a variety of fields such as telepresence, free-view videos and movies. Traditional methods [2, 16] apply 3D mesh reconstruction for this task, but the reconstructed meshes often fail to capture the complex geometry details, resulting in degraded photorealism. Neural radiance field (NeRF) [18] offers a new perspective to 3D representation, which encodes the color and geometry information of a 3D

scene with an MLP network, and performs rendering via volumetric ray-marching. Recent work [5, 21, 31] has successfully applied NeRF to animatable humans and demonstrated promising results in free view synthesis.

Nontheless we still observe non-neglectable artifacts on the NeRF generated human videos. For example, the NeRF tends to product smooth human videos, blurring the human appearance and losing high-frequency human details (e.g., garment wrinkles) [21, 22]. The state-of-the-art method [5] proposed a UV volume representation to separate the high-frequency appearance from the 3D volume, and encode them into 2D neural texture stacks. Such representation can nicely preserve the human details. However, the UV values and textures in this approach are not consistent across different poses, resulting in the synthesized appearance keeping jittering in videos (see the supplementary video for example). The NeRF-based methods also have high computational costs in the rendering process, which makes them difficult to reach real-time performance on animated humans (with the exception [5]).

In this paper, we aim to synthesize high-quality free-view human videos in new motions, both with frame-consistent appearance details and in real time. To achieve the goal, we adopt the state-of-the-art 3D Gaussian representation [14], which renders high-quality images at a faster framerate than existing NeRF-based methods via Gaussian splatting. However, extending 3D Gaussians to animatable humans is non-trivial. The 3D Gaussian splatting is designed for static scenes, and recent dynamic Gaussians [28] are proposed to *replay* a dynamic scene in a video, which are not suitable for representing humans in unseen motions.

To solve the above problems, we propose a novel animatable 3D Gaussian model. The model stores 3D Gaussians representing the human appearance in rest pose, and drives the Gaussians to target poses via a body model (i.e., SMPL) [16]. Such a model requires addressing the following challenges to be capable of synthesizing high-quality human images in new poses. First, the 3D rest-pose Gaussians are learned to fit the rest pose appearance, directly transforming them to a new pose will inevitably ruin the appearance, yielding non-neglectable artifacts such as blurring and unnatural dislocation (see Fig. 6). Second, existing Gaussian models learn the input images as a whole, while in our scenario we expect the Gaussians focus on the foreground human only to avoid the interference of background. However, simply computing the loss on the foreground cannot prevent the Gaussian from diffusing into empty spaces outside the human body, producing large artifacts (see Row 2 Column 2 in Fig. 6 for example). Third, the estimated joint parameters from images are inaccurate. We find such errors in transformation also result in apparent artifacts on synthesized images (e.g., the disappearance of hands in Row 2 Column 4 of Fig. 6).

To tackle these challenges, we augment the 3D Gaussians by attaching a learnable code on each Gaussian. Such learnable code serves as a pose-dependent appearance embedding. We also define an appearance refinement model, which takes as input the learnable code and target pose, and produces the residual Gaussian properties related to appearance. The rest-pose Gaussians are updated with the residual properties to match the target-pose appearance. To force the Gaussians to fit the foreground human only, we design a novel alpha loss in training to explicitly constrain the Gaussians within the human body, which computes the accumulated opacities of Gaussians to obtain an alpha mask, and minimizes its difference with the groundtruth human mask. We further add a human boundary mask to avoid the Gaussians to fit the zigzag areas around the boundary. To alleviate the errors caused by inaccurate pose estimation, we propose to jointly optimize the human joint rotations and positions along with the learnable codes and model parameters.

After training on multi-view videos of the human, we can synthesize high-quality free-view human videos in unseen poses with the proposed animatable 3D Gaussian model. Thanks to the learnable code, we can use a shallow MLP net while obtaining high-quality results. Consequently, the animation is performed in real time, and is much faster than the state-of-the-art NeRF-based methods (66 fps versus 18 fps in novel pose synthesis in [5]). We conduct extensive experiments on two widely-used datasets: ZJU Mocap and H36M datasets. The qualitative and quantitative results demonstrate clear improvements of our approach from existing solutions. The animatable 3D Gaussian model can well preserve high-frequency human details without frame jittering. In summary, our main contributions are as follows:

- a novel animatable 3D Gaussian model for rendering high-quality free-view human motions in real time;
- Gaussian augmentation, attaching a learnable code on each Gaussian to make the rest-pose Gaussians capable of synthesizing photorealistic images in novel poses;
- alpha loss, making the Gaussians learn the foreground human only without bringing unsatifying artifacts.

2. Related work

Novel View Synthesis for Static Scenes. Novel view synthesis for static scenes is a well-explored problem, which aims to synthesize new images from arbitrary views of a scene captured by multiple images. Traditional approaches [4, 6, 7] construct light fields to generate novel views from densely sampled images, which does not rely on any geometric estimation. Recently, Neural Radiance Field (NeRF) [18] has been a popular technique for this task, by representing a static scene with implicit fields of view-dependent color and density using a deep MLP. Although NeRF achieves high-quality novel views, its training and

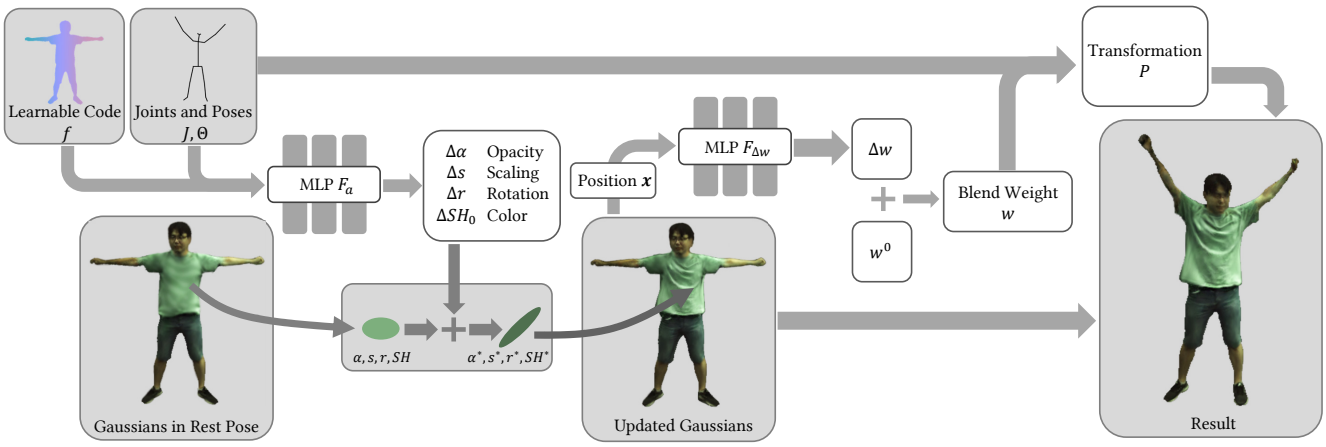

Figure 2. Overall pipeline of proposed framework. Our method uses a tiny MLP F_a to decode pose-dependent variations of 3D Gaussians from the given pose Θ and the learnable code that attached on each Gaussian. The updated Gaussians present pose-dependent effects, such as wrinkles of clothing. To transform Gaussians in rest pose to the given pose, we use the blend weight, which is sum of the initial blend weight w^0 acquired from the SMPL [16] model and the residual blend weight Δw predicted by MLP $F_{\Delta w}$. The rigid transformation P of each Gaussian can be calculated by linear blend skinning (LBS) model. The updated and transformed Gaussians are rasterized as 3DGS [14] to synthesize the final result.

rendering is time-consuming. Subsequent work [8, 19, 29] attempts different strategies to accelerate NeRF. For example, instant-ngp [19] replaces the deep MLP by a shallow MLP with the multiresolution hash encoding as input, which can be trained in a few minutes and render images in real-time. Recently, 3D gaussian splatting (3DGS) [14] has demonstrated the strong ability of explicit representation in novel view synthesis tasks. 3DGS builds an differentiable rasterizer to optimize the position, covariance and appearance of 3D Gaussians from image loss. Compared to NeRF-based methods which depend on expensive ray marching, 3DGS utilizes traditional rasterization pipelines, which achieves more than 100 fps rendering. In addition, the explicit representation provides a more intuitive way for animation control, which motivates us to extend 3DGS to dynamic and drivable digital humans.

Free-View Human Avatar Synthesis. In the last decade, many efforts have been made to build animatable human avatars. Some work attempts to build statistical mesh template [13, 16, 20] to model human bodies. To handle the color, traditional methods scan the human to get textures and material parameters [2, 30]. For the deformable parts such as loose garments, physical simulation [9], blending from database [26] or deformation space modeling [10] is performed to improving fidelity. In the past three years, lots of works leverage neural representation to depict dynamic scenes or human avatars, including voxels [15], point clouds [25], neural textures [3, 17], and NeRF [21, 27, 31]. Animatable NeRF [21] uses SMPL [16] to establish correspondences between arbitrary poses and the rest pose, and model the pose-dependent details by conditioning the MLP on learnable appearance codes of each frame. However, the appearance code needs to be optimized for any given novel pose, which reduces its pose generalization ability. To model more local details, Zheng et al. [32] assemble the radiance field of dynamic avatars by a set of local ones, which improves visual quality of garment wrinkles. However, these methods based on neural representation suffer from slow training and rendering. Fourier PlenOctrees [24] utilizes Fourier transformation to compact the dynamic octrees of the scene in time domain, which realizes 100 fps rendering but without the ability of novel pose generation. InstantAvatar [12] incorporates instant-ngp in avatar learning and achieves 15 fps performance, but they focus on the monocular video input which is beyond our scope. As the NeRF-based methods generate smooth results losing details, UV Volume [5] instead renders a UV map by neural volume rendering and uses a generator to obtain the textures conditioned on the pose. UV Volume can render high quality appearance with high-frequency details, and also reaches real-time rendering, but its UV and texture prediction is inconsistent across video frames, causing jittering human appearances in videos. Different from NeRF-based approaches, our method directly applies the SMPL model to explicitly transform the 3D Guassians and distributes a learnable appearance code to each Gaussian, which is decoded by a tiny MLP to obtain pose-dependent human appearances. Our method produces high quality video results and also keeps high real-time performance.

3. Approach

3.1. Overview

We aim to reconstruct an animatable 3D Gaussian model for a person from a multi-view video, so that we can synthesize photorealistic videos for the person in novel poses under novel views. To achieve the goal, we propose a augmented Gaussian model by attaching a learnable code f on each Gaussian. Such Gaussian model can well fit the input frames in different poses, and generalize well to the person in unseen poses (Sec. 3.2). We further present how to learn the representation on the multi-view video (Sec. 3.3). The pipeline of our work is shown in Fig. 2.

3.2. Representing Dynamic Humans with 3D Gaussians

3D Gaussians are a novel representation of radiance fields [14]. Each Gaussian maintains the properties of 3D position, opacity, anisotropic covariance, and spherical harmonic (SH) coefficients. Then a static scene can be realistically rendered with anisotropic splatting.

To extend 3D Gaussians to animatable humans, a straightforward approach is to adopt the SMPL model [16] to transform the the rest-pose Gaussians to the target pose. However, such geometric transformation will ruin the Gaussians' capacity of synthesizing high-quality appearances, resulting in non-neglectable artifacts such as blurring and joint dislocation. To this end, we attach a learnable code f to each Gaussian in rest pose. The learnable code serves as a pose-dependent appearance embedding for eliminating the appearance errors of transformed Gaussians.

Specifically, given the rest-pose Gaussian model $\{G_i\}$ where G_i is a 3D Gaussian containing position $\mathbf{x}_i$, opacity α_i, scale $\mathbf{s}_i$, rotation r_i, spherical harmonics SH_i and learnable code f_i, for a target pose $\Theta \in \mathbb{R}^{K\times 3}$ represented as rotations of K joints, we define a pose-dependent appearance refinement model F_a as:

$$\{\Delta\alpha_i, \Delta\mathbf{s}_i, \Delta r_i, \Delta SH_{i0}\} = F_a(\Theta, f_i). \tag{1}$$

The Gaussian properties are updated accordingly (with position unchanged) as

$$\begin{aligned} \alpha_i^* = \alpha_i + \Delta\alpha_i, \mathbf{s}_i^* = \mathbf{s}_i + \Delta\mathbf{s}_i, R_i^* = \Delta r_i r_i, \\ SH_i^* = \{SH_{i0} + \Delta SH_{i0}, SH_{i1}, SH_{i2}, SH_{i3}\}. \end{aligned} \tag{2}$$

We find that continuous optimization of higher-order spherical harmonics tend to make ambiguity between pose-dependent and view-dependent variations, which reduces the ability of novel view or novel pose generation, especially in the case of sparse training input. Therefore, we only update the zero-order spherical harmonics (view-independent color) to avoid overfitting and accelerate training and rendering.

After obtaining the updated Gaussians in rest pose, we can transform the Gaussians to render the photo-realistic image for target pose. We utilize the SMPL human model [16] for this task. The human skeleton has K parts with K transformation matrices $P_k \in SE(3)$ (computed from the joint rotations Θ_k and joint positions J_k). For a Gaussian G_i in rest pose, its corresponding transformation is

$$P_i = \sum_{k=1}^{K} w_k(\mathbf{x}_i) P_k. \tag{3}$$

We take the strategy in [21] to compute the blend weights w. We project $\mathbf{x}_i$ to the SMPL mesh surface in rest pose, and the initial blend weights w^0 are obtained using barycentric interpolation of the weights of corresponding triangle vertices. Such initial weights are inaccurate. Hence we apply a positional encoded MLP network to predict residual weights $F_{\Delta w} : \mathbf{x} \rightarrow \Delta w(\mathbf{x})$, and the final blend weights are computed as $w(\mathbf{x}_i) = w^0(\mathbf{x}_i) + F_{\Delta w}$.

The transformation P_i for each Gaussian is further decomposed to scale S_i, rotation R_i and translation T_i [23]. We omit the shear component to prevent the Gaussian from distortion. In this way, the Gaussians are transformed as

$$\begin{aligned} \mathbf{x}_i^t = R_i\mathbf{x}_i^* + T_i, \mathbf{s}_i^t = S_i\mathbf{s}_i^*, r_i^t = R_i r_i^*, \\ SH_i^t = SH\_Rotation(R_i, SH_i^*). \end{aligned} \tag{4}$$

Here for the rotation of SH $SH\_Rotation$, directly rotating spherical harmonics is inefficient. A better approach is to inversely rotate view directions. Specifically, we first calculate the direction from the camera center to the gaussian position as the view direction, and then we apply the inverse rotation transformation to view directions as the input for SH evaluation.

Finally, we are able to render the high-quality images of the human in target pose with the transformed Gaussians $\{G_i^t\}$. We apply the same rasterizer as [14] to perform differentiable rendering and obtain the rendered image I_{render}.

3.3. Training

Based on the dynamic 3D Gaussians $\{G_i^t\}$, we can synthesize the human image of particular pose and view for each video frame. The learnable code $\{f_i\}$, as well as the parameters of F_a and $F_{\Delta w}$ are jointly optimized over the multi-view video by minimizing the L_1 difference between the rendered image I_{render} and the video frame I_{gt}. Note that the joint rotations Θ and joint positions J estimated from SMPL are not perfect, so we also optimize Θ and J. We make use of a human boundary mask M_b when computing the image loss. The boundary mask sets the human boundary areas (5 pixels) 0 while all other areas 1. We find this simple approach can effectively avoid the Gaussians to fit

the zigzags around the boundaries. The image loss is defined as

$$L_{rgb} = \sum_{j=1}^{F}(||(I^j_{render} - I^j_{gt}) \odot M_b||), \tag{5}$$

where F is the frame number and $\odot$ is the pixelwise multiplication. λ is 0.2 in all our experiments.

In order to alleviate the background interference when learning the Gaussians, a simple way is to only compute the image loss on the foreground human using the image mask M_h. However, we found this option will cause Gaussians to grow out of the human. Moreover, when generating novel views, Gaussians with the same color as the background will occlude parts of the body. To overcome these problems, we design a novel alpha loss to compare the rendered opacity image with the mask M_h. Specifically, we set all the SHs to pure white and perform rendering. In this way we obtain the accumulated opacity image $I_{opacity}$. The alpha loss is defined as:

$$L_\alpha = \sum_{j=1}^{F}(||(I^j_{opacity} - M^j_h) \odot M_b||_2). \tag{6}$$

We also add a blend weight loss to constrain the Gaussians from being stretched too long or too big, which will cross the joints and yield artifacts in novel poses, especially in sparse training input. Specifically, for each Gaussian G_i, its scale $\mathbf{s}$ corresponds to 3 scales $\{s_1, s_2, s_3\}$ along the Gaussian axes $\{\mathbf{a}_1, \mathbf{a}_2, \mathbf{a}_3\}$. we fetch 6 points along the 3 axes: $\mathbf{p}_i^{\pm l \in 1,2,3} = \mathbf{x_i} \pm s_l \mathbf{a}_l$, and compute their corresponding blend weights $\{w(\mathbf{p}_i^{\pm 1}), w(\mathbf{p}_i^{\pm 2}), w(\mathbf{p}_i^{\pm 3})\}$. The blend weight loss is defined as the standard deviations of the 6 weights on all Gaussians:

$$L_w = \sum_{i=i}^{n} \mathrm{std}(\mathrm{w}(\mathbf{p}_\mathrm{i}^{\pm 1}), \mathrm{w}(\mathbf{p}_\mathrm{i}^{\pm 2}), \mathrm{w}(\mathbf{p}_\mathrm{i}^{\pm 3})). \tag{7}$$

We also follow [14] to add a D-SSIM term in the loss function. The overall loss function is defined as:

$$L = \lambda_1 L_{rgb} + \lambda_2 L_\alpha + \lambda_3 L_w + \lambda_4 L_{D-SSIM}, \tag{8}$$

where we set $\lambda_1 = 0.8, \lambda_2 = 10, \lambda_3 = 0.2, \lambda_4 = 0.2$ in all our tests.

3.4. Implementation Details

We adopt shallow 4-layers MLPs with ReLU activations for both F_a and $F_{\Delta w}$. The hidden layer width of the MLP F_a and $F_{\Delta w}$ is 128 and 32, respectively. The dimension of the learnable code f is 9, which is initialized to positional encoding at the beginning.

To enhance the training stability and improve the generalization ability, we divide our training process into two stages. In the initialization stage (first 5000 iterations), we disable the pose-dependent appearance refinement model F_a and residual weights prediction MLP $F_{\Delta w}$, and only optimize rest-pose Gaussians, as well as joint parameters in target poses, which is equivalent to obtaining an average human model. The initialization stage provides a good reference for subsequent optimization. In the fine-tuning stage (after 5000 iterations), we enable these two MLPs to fit the pose-dependent details, and the Gaussians and joint parameters are still jointly optimized. It should also be noted that in Eq. (1), we stop the gradient of Θ to disentangle poses from the appearance information.

To avoid training falling into local optima, we reset the opacities of Gaussians every fixed number of iterations, similar to 3DGS [14]. In the initialization stage, we reset the opacity at the 3000th iteration. In the fine-tuning stage, we reset the opacity every 6000 iterations. We apply a similar Gaussian densification and pruning strategy as in 3DGS, but the difference is that we use the sum of the gradiants from the alpha and RGB loss to determine whether to densify Gaussians, which accelerates the fitting of deformable garments. In addition, we use the scales and opacities of Gaussians in rest pose (i.e. without the updated values from F_a) to split or prune Gaussians, which keeps the consistency across all poses.

4. Experiments

All experiments are conducted on a workstation with an i7-13700KF CPU, 32GB memory and an NVIDIA RTX 4090 GPU. To show the effectiveness and efficiency of our approach, we conduct comprehensive experiments. We present quantitative results measured with four standard metrics: PSNR, SSIM, LPIPS, and FPS. Note that we use the whole image including the black background instead of the masked image for metric evaluation, so the results are better than the reported results for those compared NeRF-based methods, which evaluate metrics by the color of rays and the corresponding pixels of the ground-truth (without background). We also present the qualitative results to further illustrate that our method is able to generate high fidelity human avatars with garments in novel view and novel pose synthesis tasks.

Dataset. We perform experiments on ZJU Mocap dataset [22] and H36M dataset [11], which include multi-view sequences, calibrated camera parameters, masks and poses (estimated by EasyMocap [1]). We use 20 training views on ZJU Mocap dataset with 512×512 resolution. To test our method under sparse input conditions, we only use 3 views for training on H36M dataset with 1000×1000 resolution.

Baselines. We validate our method by comparing it with several state-of-the-art human avatar synthesis methods: 1) AN: Animatable NeRF [21], which projects points in a

given pose to the canonical space (rest pose) by the blend weight fields based on the SMPL [16] model, and renders the human following the NeRF pipeline; 2) UV: UV Volume [5], which generates the UV map by volume rendering and use CNNs to obtain pose-dependent textures.

Efficiency. Tab. 1 shows the comparison of our method with baselines in terms of efficiency. Given a novel pose, Animatable NeRF needs to generate the blend weight field from the SMPL model and optimize the corresponding appearance latent code, which is actually not comparable in real-time performance. Our method achieves the highest FPS, which enables real-time rendering on both novel view and novel pose synthesis tasks. Especially in the task of novel view synthesis, we can cache the MLP outputs to reach the same FPS reported in 3DGS [14]. Our method attaches a learnable code to each Gaussian and decodes it by a tiny MLP, which accelarate the rendering without sacrificing the visual quality. In addition, the training of our method can fully converge within 2 hours, while the baselines need the training time of more than 10 hours.

Methods	AN [21]	UV [5]	Ours
Novel View Synthesis	3 fps	52 fps	114 fps
Novel Pose Synthesis	0.06 fps	18 fps	66 fps

Table 1. Comparison of rendering efficiency with Animatable NeRF (AN) [21] and UV Volume (UV) [5].

Novel View Synthesis. We synthesize images of training poses in test views. The quantitative results are shown in Tab. 2. In most cases, our method shows the best PSNR and SSIM, while the LPIPS of UV Volume is better than ours on ZJU Mocap dataset. However, the synthesized details from UV Volume can be quite different from the ground truth (see Fig. 1), leading to fake wrinkles. More importantly, we observe the UV and texture prediction of UV Volume is inconsistent across video frames, resulting in appearant jitter artifacts (please see the supplmentary video). In the H36M dataset, Our method is significantly superior to the baseline in terms of PSNR, which shows our good generalization ability in the case of sparse input for training.

Fig. 3 presents the qualitative comparisons. Animatable NeRF fails to preserve high-frequency details and some parts of the body can even disappear. UV Volume does exhibit abundant texture and wrinkle details, but as mentioned above, they can differ from the ground-truth and jitter across frames. Moreover, UV Volume exists small split parts and aliasing artifacts on the boundary. Our method faithfully present details of clothing wrinkles and garments away from the human body. Our method even eliminate zigzags resulting from binary masks compared to the ground-truth.

Novel Pose Synthesis. We synthesize images of training views in test poses. The quantitative results are shown in Tab. 3. Similar to the novel view synthesis, our method achieves the best PSNR and SSIM, while the LPIPS is slightly higher than UV Volume. Compared with novel view synthesis, our method has greater advantages in novel pose synthesis.

The qualitative comparisons are shown in Fig. 4. There are more artifacts for UV Volume in the task of novel pose synthesis, such as odd clothing wrinkles and arms of varying widths. Our method preserves detailed spatially-varying textures of clothes and always synthesizes robust shapes of body and limbs. In general, our method performs better in the novel pose synthesis task, and is better than baselines in both the novel view and pose synthesis tasks.

Temporal Stability. One of the most important applications of human avatars is to generate continuous videos. The temporal jittering seriously affects the visual effects. For a more intuitive comparison of the temporal stability, we calculate the error map between two adjacent frames of a action sequence. Note that the error map of the ground-truth is not all 0. Therefore, we show the error maps of our results, baselines and the ground-truth in Fig. 5, which proves that our method has the best temporal stability. Although UV Volume achieves clear and high-frequency textures by CNNs, temporal jittering is still a common problem in these generative models.

4.1. Ablation Studies

We conduct ablation studies on sequence 313 of the ZJU Mocap dataset. We validate the impacts of some possible options, including using the positional encoding as the input of F_a instead of the leanable code, only computing image loss in the masked region, and updating the higher-order spherical harmonics with F_a. Moreover, we also validate the necessity of some modules by removing the optimization of joint parameters, appearance MLP F_a, boundary mask, alpha loss and blend weight loss, respectively. The quantitative results are shown in Sec. 4.1 and the qualitative results are illustrated in Fig. 6.

Postional encoding versus learnable code. Attaching a learnable code to each Gaussian to learn the appearance variations among different poses can synthesize higher quality images. In contrast, using positional encoding as the MLP input leads to lack of details. Using longer positional encoding or deeper MLP may alleviate this problem but severely reduce the real-time performance.

Image loss from the masked region only versus from the whole image. Different from the NeRF based methods, 3D Gaussians splat colors within a region. If we only compute the image loss from the masked region, some Gaussians will be optimized out of the human region but still contribute to the final result, which will cause artifacts outside humans in novel views or novel poses. In contrast, our alpha loss explicitly constrains the Gaussians within human

Datasets		ZJU								H36M						
		313	315	377	386	387	390	392	394	s1p	s5p	s6p	s7p	s8p	s9p	s11p
PSNR ↑	AN [21]	30.42	28.61	30.45	34.33	31.11	35.47	32.54	31.23	28.66	29.67	29.42	29.51	28.12	29.44	28.88
	UV [5]	32.20	28.87	31.96	36.61	31.16	36.26	32.49	33.20	28.80	30.12	29.50	29.49	28.50	29.25	29.07
	Ours	33.32	30.50	31.75	37.97	32.42	37.41	33.21	34.21	33.10	34.76	33.16	33.73	32.29	33.14	34.25
SSIM ↑	AN	0.963	0.969	0.985	0.971	0.977	0.965	0.966	0.961	0.984	0.983	0.978	0.979	0.979	0.964	0.980
	UV	0.977	0.979	0.980	0.987	0.977	0.988	0.976	0.977	0.981	0.985	0.977	0.984	0.982	0.977	0.981
	Ours	0.990	0.989	0.985	0.993	0.988	0.994	0.983	0.987	0.992	0.994	0.991	0.994	0.992	0.990	0.992
LPIPS ↓	AN	0.041	0.034	0.044	0.036	0.040	0.027	0.061	0.052	0.026	0.023	0.029	0.024	0.026	0.028	0.033
	UV	0.029	0.021	0.028	0.018	0.027	0.016	0.032	0.029	0.025	0.021	0.026	0.021	0.027	0.028	0.031
	Ours	0.036	0.030	0.037	0.026	0.041	0.021	0.054	0.046	0.024	0.021	0.027	0.020	0.024	0.027	0.028

Table 2. Quantitative results of novel view synthesis. Our method outperforms baselines (AN: Animatable NeRF [21], UV: UV Volume [5]) on PSNR and SSIM and present competitive LPIPS.

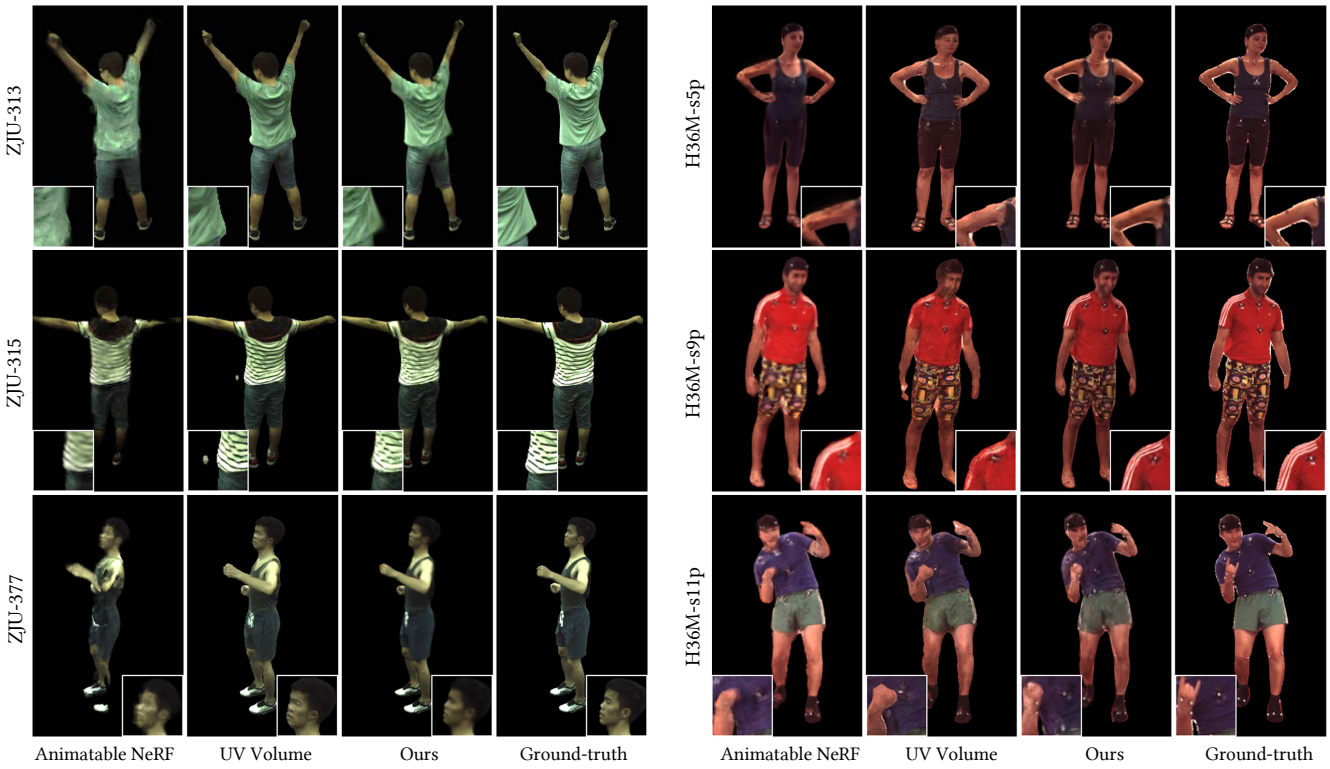

Figure 3. Qualitative results of novel view synthesis on ZJU Mocap and H36M datasets. Our method produces high-fidelity images with wrinkles and stripes on clothes. Animatable NeRF [21] produces blurred details and empty holes in some cases (ZJU-313 and ZJU-377). UV Volume [5] presents clear and sharp details in most cases, but tend to generate unstable shape of boundary (H36M-s5p) or split parts (ZJU-315).

regions.

Updating all-order versus zero-order spherical harmonics. Compared to 3DGS [14], transformation from poses increase the degrees of freedom. To disentangle pose-dependent and view-dependent appearance variations, we only update the zero-order spherical harmonics related to pose transformation by F_a. As illustrated in Fig. 6, updating all-order spherical harmonics leads to more noisy results due to overfitting.

Necessity of optimization of joint parameters. The joint parameters provided by the dataset are estimated by EasyMocap [1], which can not be totally accurate. Inaccurate joint positions causes unsmooth bending of joints and inaccurate joint rotations leads to blurring.

Necessity of the boundary mask. Gaussian splatting has smooth color fade, while the binary masks have aliasing

Datasets		ZJU								H36M						
		313	315	377	386	387	390	392	394	s1p	s5p	s6p	s7p	s8p	s9p	s11p
PSNR ↑	AN [21]	30.81	28.24	31.43	35.20	29.55	33.88	31.32	31.61	31.34	32.66	32.15	30.24	30.88	31.47	31.85
	UV [5]	30.75	28.30	31.20	34.92	29.62	34.44	31.51	31.14	30.38	31.84	30.96	30.27	30.95	30.92	30.61
	Ours	33.41	30.17	32.13	36.85	31.76	35.57	32.76	32.79	37.86	36.77	35.86	36.63	36.48	37.39	38.44
SSIM ↑	AN	0.971	0.973	0.981	0.969	0.975	0.970	0.970	0.989	0.990	0.988	0.986	0.983	0.985	0.991	0.990
	UV	0.968	0.974	0.979	0.984	0.972	0.985	0.971	0.968	0.988	0.988	0.984	0.987	0.987	0.987	0.988
	Ours	0.988	0.988	0.986	0.992	0.987	0.993	0.983	0.984	0.997	0.996	0.995	0.996	0.997	0.996	0.997
LPIPS ↓	AN	0.042	0.033	0.038	0.032	0.044	0.028	0.062	0.055	0.022	0.020	0.019	0.021	0.016	0.018	0.024
	UV	0.039	0.024	0.030	0.020	0.030	0.017	0.039	0.036	0.019	0.017	0.018	0.017	0.017	0.018	0.022
	Ours	0.036	0.030	0.040	0.030	0.045	0.026	0.057	0.052	0.013	0.017	0.018	0.014	0.013	0.015	0.015

Table 3. Quantitative results of novel pose synthesis. Our method outperforms baselines (AN: Animatable NeRF [21], UV: UV Volume [5]) on PSNR and SSIM (especially on H36M dataset) and present competitive LPIPS.

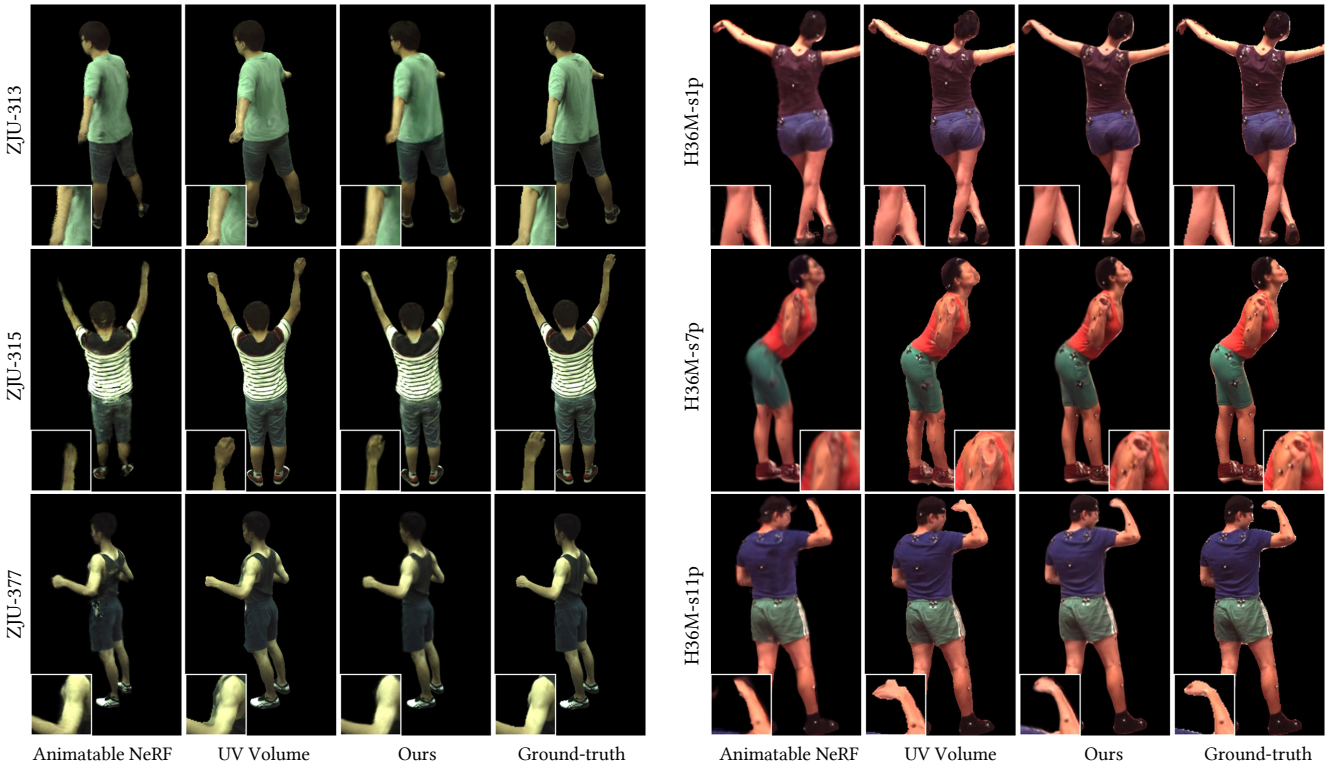

Figure 4. Qualitative results of novel pose synthesis on ZJU Mocap and H36M datasets. Our method produces high-fidelity and anti-aliasing synthesis results, even if there are aliasing problems in the ground-truth. Animatable NeRF [21] produces blurred results and the human's arm sometimes disappear (ZJU-315). UV Volume [5] produces fake wrinkles (ZJU-313), unstable shape of boundary (ZJU-315, H36M-s1p and H36M-s11p) and ghosting (ZJU-377) in some cases.

and mutation on the boundary. If we force Gaussians to fit the masked image, lots of tiny Gaussians will be generated to make the boundary harder. In our experiment, the number of Gaussians is four times that of using the boundary mask. More Gaussians do not provide higher quality, but rather noise.

Impacts of F_a and losses. Without the appearance refinement model F_a, the result is just the average colors of all poses. Alpha loss not only constrains the position of Gaussians and removes the background interference, but also makes our method more sensitive to the movement of garments. Blend weight loss limits the anisotropy of Gaussians, which prevents Gaussians from protruding in novel poses.

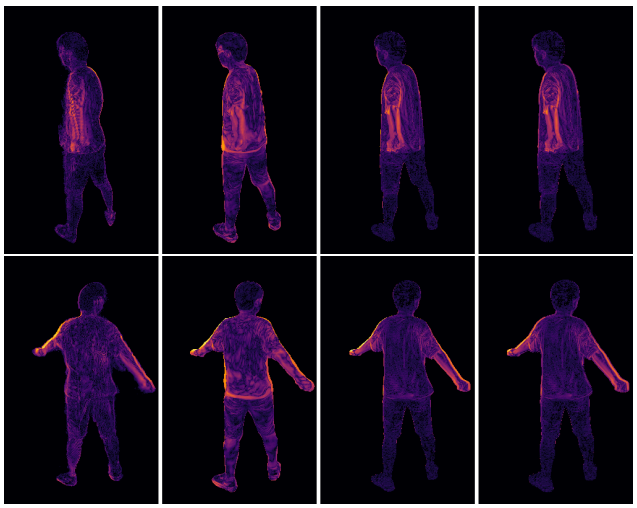

Figure 5. Error maps between two adjacent frames of a action sequence. Compared to the ground-truth, the error maps of UV Volume [5] shows the largest error on the boundary, which is the main reason for temporal jittering.

Ablations	Novel View Synthesis			Novel Pose Synthesis		
	PSNR ↑	SSIM ↑	LPIPS ↓	PSNR ↑	SSIM ↑	LPIPS ↓
Complete Model	33.32	0.989	0.036	33.41	0.987	0.036
Original 3DGS [14]	28.56	0.976	0.083	29.56	0.976	0.081
Positional Encoding	30.03	0.981	0.053	30.32	0.978	0.053
Only Foreground	24.22	0.291	0.163	24.26	0.280	0.160
All-order SH	33.31	0.989	0.038	32.73	0.986	0.039
No Joints Optim.	32.42	0.986	0.053	32.19	0.984	0.051
No Boundary Mask	32.10	0.986	0.044	32.41	0.984	0.044
No F_a	29.50	0.981	0.075	29.99	0.979	0.073
No L_α	33.21	0.988	0.040	32.01	0.985	0.042
No L_w	33.32	0.989	0.041	33.04	0.986	0.043

Table 4. Ablation study about possible options and the necessity of some modules. "Only Foreground" means only computing image loss from the masked region. "All-order SH" means updating all-order SH by F_a in the fine-tuning stage. "No Joints Optim." means no optimization of poses and joints.

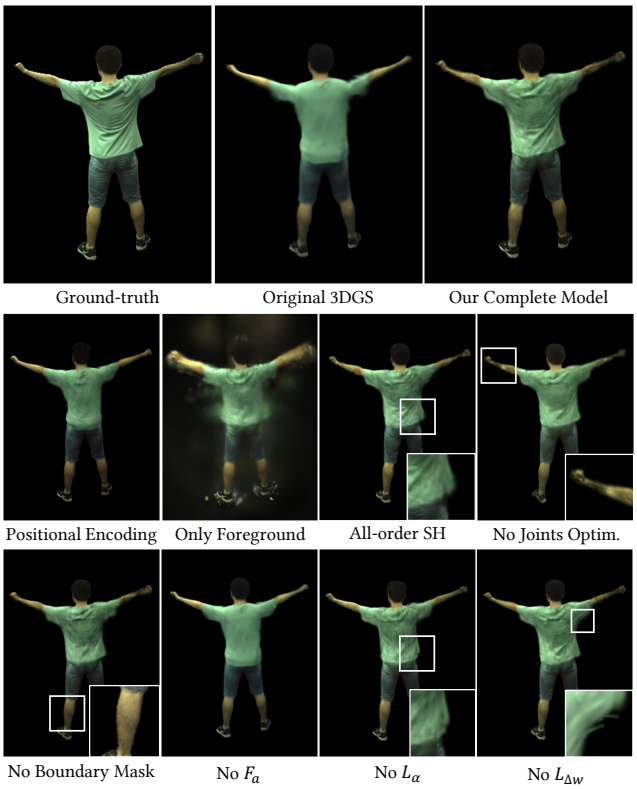

Figure 6. Visualization of ablations. Directly applying 3DGS [14] to human avatars (Original 3DGS) leads to blurring and joint dislocation. Using positional encoding instead of the learnable code or not using F_a also lead to blurring. Only computing image loss from the masked region (Only Foreground) causes Gaussian to splat in empty spaces. Updating all-order SH by F_a (All-order SH) decrease the efficiency of training and rendering, and also causes noise and some artifacts in novel view due to overfitting. Without joints and poses optimization, hands may disappear in some cases. Without the boundary mask, noise and zigzags on boundary appear. Without alpha loss L_α, the movement of garment disappears. Without the blend weight loss $L_{\Delta w}$, some Gaussians protrude in nove pose.

4.2. Limitation

Our method is able to synthesize robust, high quality and temporally stable human avatars in both novel views and novel poses. However, when the training view is too sparse, our method tends to overfit and generates low quality results in novel view. Besides, when the wrinkles of garment change greatly, our method may produce a transition with observable noise. Adding more constraints or introducing prior information may alleviate these problems.

5. Conclusions

We present a novel animatable 3D Gaussian model for rendering high-quality free-view human motions in real time. It can well synthesize high-frequency and frame-consistent appearance details. We make non-trivial efforts to adapt the original 3D Gaussian model to the animatable humans, including attaching learnable codes to Gaussians to refine apperance errors caused by transformation, designing a new alpha loss to explict constrain the Gaussians within the human body, and jointly optimizing the human joint parameters. Experiments on the ZJU-MoCap and H36M datasets demonstrate that our model achieves state-of-the-art performance on video synthesis under novel views and novel human poses.

References

[1] Easymocap - make human motion capture easier. Github, 2021. 5, 7

[2] Brett Allen, Brian Curless, and Zoran Popović. The space of human body shapes: reconstruction and parameterization from range scans. *ACM transactions on graphics (TOG)*, 22 (3):587–594, 2003. 1, 3

[3] Timur Bagautdinov, Chenglei Wu, Tomas Simon, Fabian Prada, Takaaki Shiratori, Shih-En Wei, Weipeng Xu, Yaser Sheikh, and Jason Saragih. Driving-signal aware full-body avatars. *ACM Transactions on Graphics (TOG)*, 40(4):1–17, 2021. 3

[4] Chris Buehler, Michael Bosse, Leonard McMillan, Steven Gortler, and Michael Cohen. Unstructured lumigraph rendering. In *Seminal Graphics Papers: Pushing the Boundaries, Volume 2*, pages 497–504. 2023. 2

[5] Yue Chen, Xuan Wang, Xingyu Chen, Qi Zhang, Xiaoyu Li, Yu Guo, Jue Wang, and Fei Wang. Uv volumes for real-time rendering of editable free-view human performance. In *Proceedings of the IEEE/CVF Conference on Computer Vision and Pattern Recognition*, pages 16621–16631, 2023. 2, 3, 6, 7, 8, 9

[6] Abe Davis, Marc Levoy, and Fredo Durand. Unstructured light fields. In *Computer Graphics Forum*, pages 305–314. Wiley Online Library, 2012. 2

[7] Martin Eisemann, Bert De Decker, Marcus Magnor, Philippe Bekaert, Edilson De Aguiar, Naveed Ahmed, Christian Theobalt, and Anita Sellent. Floating textures. In *Computer graphics forum*, pages 409–418. Wiley Online Library, 2008. 2

[8] Stephan J Garbin, Marek Kowalski, Matthew Johnson, Jamie Shotton, and Julien Valentin. Fastnerf: High-fidelity neural rendering at 200fps. In *Proceedings of the IEEE/CVF International Conference on Computer Vision*, pages 14346–14355, 2021. 3

[9] Peng Guan, Loretta Reiss, David A Hirshberg, Alexander Weiss, and Michael J Black. Drape: Dressing any person. *ACM Transactions on Graphics (ToG)*, 31(4):1–10, 2012. 3

[10] Marc Habermann, Lingjie Liu, Weipeng Xu, Michael Zollhoefer, Gerard Pons-Moll, and Christian Theobalt. Real-time deep dynamic characters. *ACM Transactions on Graphics (ToG)*, 40(4):1–16, 2021. 3

[11] Catalin Ionescu, Dragos Papava, Vlad Olaru, and Cristian Sminchisescu. Human3. 6m: Large scale datasets and predictive methods for 3d human sensing in natural environments. *IEEE transactions on pattern analysis and machine intelligence*, 36(7):1325–1339, 2013. 5

[12] Tianjian Jiang, Xu Chen, Jie Song, and Otmar Hilliges. Instantavatar: Learning avatars from monocular video in 60 seconds. In *Proceedings of the IEEE/CVF Conference on Computer Vision and Pattern Recognition*, pages 16922–16932, 2023. 3

[13] Hanbyul Joo, Tomas Simon, and Yaser Sheikh. Total capture: A 3d deformation model for tracking faces, hands, and bodies. In *Proceedings of the IEEE conference on computer vision and pattern recognition*, pages 8320–8329, 2018. 3

[14] Bernhard Kerbl, Georgios Kopanas, Thomas Leimkühler, and George Drettakis. 3d gaussian splatting for real-time radiance field rendering. *ACM Transactions on Graphics (ToG)*, 42(4):1–14, 2023. 2, 3, 4, 5, 6, 7, 9

[15] Stephen Lombardi, Tomas Simon, Jason Saragih, Gabriel Schwartz, Andreas Lehrmann, and Yaser Sheikh. Neural volumes: Learning dynamic renderable volumes from images. *arXiv preprint arXiv:1906.07751*, 2019. 3

[16] Matthew Loper, Naureen Mahmood, Javier Romero, Gerard Pons-Moll, and Michael J Black. Smpl: A skinned multi-person linear model. In *Seminal Graphics Papers: Pushing the Boundaries, Volume 2*, pages 851–866. 2023. 1, 2, 3, 4, 6

[17] Shugao Ma, Tomas Simon, Jason Saragih, Dawei Wang, Yuecheng Li, Fernando De La Torre, and Yaser Sheikh. Pixel codec avatars. In *Proceedings of the IEEE/CVF Conference on Computer Vision and Pattern Recognition*, pages 64–73, 2021. 3

[18] Ben Mildenhall, Pratul P. Srinivasan, Matthew Tancik, Jonathan T. Barron, Ravi Ramamoorthi, and Ren Ng. Nerf: Representing scenes as neural radiance fields for view synthesis. In *ECCV*, 2020. 1, 2

[19] Thomas Müller, Alex Evans, Christoph Schied, and Alexander Keller. Instant neural graphics primitives with a multiresolution hash encoding. *ACM Transactions on Graphics (ToG)*, 41(4):1–15, 2022. 3

[20] Ahmed AA Osman, Timo Bolkart, and Michael J Black. Star: Sparse trained articulated human body regressor. In *Computer Vision–ECCV 2020: 16th European Conference, Glasgow, UK, August 23–28, 2020, Proceedings, Part VI 16*, pages 598–613. Springer, 2020. 3

[21] Sida Peng, Junting Dong, Qianqian Wang, Shangzhan Zhang, Qing Shuai, Xiaowei Zhou, and Hujun Bao. Animatable neural radiance fields for modeling dynamic human bodies. In *Proceedings of the IEEE/CVF International Conference on Computer Vision*, pages 14314–14323, 2021. 2, 3, 4, 5, 6, 7, 8

[22] Sida Peng, Yuanqing Zhang, Yinghao Xu, Qianqian Wang, Qing Shuai, Hujun Bao, and Xiaowei Zhou. Neural body: Implicit neural representations with structured latent codes for novel view synthesis of dynamic humans. In *Proceedings of the IEEE/CVF Conference on Computer Vision and Pattern Recognition*, pages 9054–9063, 2021. 2, 5

[23] Ken Shoemake and Tom Duff. Matrix animation and polar decomposition. In *Proceedings of the conference on Graphics interface*, pages 258–264, 1992. 4

[24] Liao Wang, Jiakai Zhang, Xinhang Liu, Fuqiang Zhao, Yanshun Zhang, Yingliang Zhang, Minye Wu, Jingyi Yu, and Lan Xu. Fourier plenoctrees for dynamic radiance field rendering in real-time. In *Proceedings of the IEEE/CVF Conference on Computer Vision and Pattern Recognition*, pages 13524–13534, 2022. 3

[25] Minye Wu, Yuehao Wang, Qiang Hu, and Jingyi Yu. Multi-view neural human rendering. In *Proceedings of the IEEE/CVF Conference on Computer Vision and Pattern Recognition*, pages 1682–1691, 2020. 3

[26] Feng Xu, Yebin Liu, Carsten Stoll, James Tompkin, Gaurav Bharaj, Qionghai Dai, Hans-Peter Seidel, Jan Kautz, and

Christian Theobalt. Video-based characters: creating new human performances from a multi-view video database. In *ACM SIGGRAPH 2011 papers*, pages 1–10. 2011. 3

[27] Gengshan Yang, Minh Vo, Natalia Neverova, Deva Ramanan, Andrea Vedaldi, and Hanbyul Joo. Banmo: Building animatable 3d neural models from many casual videos. In *Proceedings of the IEEE/CVF Conference on Computer Vision and Pattern Recognition*, pages 2863–2873, 2022. 3

[28] Ziyi Yang, Xinyu Gao, Wen Zhou, Shaohui Jiao, Yuqing Zhang, and Xiaogang Jin. Deformable 3d gaussians for high-fidelity monocular dynamic scene reconstruction. *arXiv preprint arXiv:2309.13101*, 2023. 2

[29] Alex Yu, Ruilong Li, Matthew Tancik, Hao Li, Ren Ng, and Angjoo Kanazawa. Plenoctrees for real-time rendering of neural radiance fields. In *Proceedings of the IEEE/CVF International Conference on Computer Vision*, pages 5752–5761, 2021. 3

[30] Chao Zhang, Sergi Pujades, Michael J Black, and Gerard Pons-Moll. Detailed, accurate, human shape estimation from clothed 3d scan sequences. In *Proceedings of the IEEE Conference on Computer Vision and Pattern Recognition*, pages 4191–4200, 2017. 3

[31] Fuqiang Zhao, Wei Yang, Jiakai Zhang, Pei Lin, Yingliang Zhang, Jingyi Yu, and Lan Xu. Humannerf: Efficiently generated human radiance field from sparse inputs. In *Proceedings of the IEEE/CVF Conference on Computer Vision and Pattern Recognition*, pages 7743–7753, 2022. 2, 3

[32] Zerong Zheng, Han Huang, Tao Yu, Hongwen Zhang, Yandong Guo, and Yebin Liu. Structured local radiance fields for human avatar modeling. In *Proceedings of the IEEE/CVF Conference on Computer Vision and Pattern Recognition*, pages 15893–15903, 2022. 3